Neuroprotective role of Sirt1 in mammalian models of Huntington's disease through activation of multiple Sirt1 targets

Mali Jiang[1,17], Jiawei Wang[1,2,17], Jinrong Fu[1], Lin Du[3], Hyunkyung Jeong[4], Tim West[5], Lan Xiang[1], Qi Peng[1], Zhipeng Hou[6], Huan Cai[7], Tamara Seredenina[8], Nicolas Arbez[1], Shanshan Zhu[1], Katherine Sommers[1], Jennifer Qian[1], Jiangyang Zhang[6], Susumu Mori[6], X William Yang[9], Kellie L K Tamashiro[10], Susan Aja[11], Timothy H Moran[10], Ruth Luthi-Carter[8], Bronwen Martin[7], Stuart Maudsley[12], Mark P Mattson[12], Robert H Cichewicz[3], Christopher A Ross[1,13–16], David M Holtzman[5], Dimitri Krainc[4] & Wenzhen Duan[1,16]

Huntington's disease is a fatal neurodegenerative disorder caused by an expanded polyglutamine repeat in huntingtin (HTT) protein. We previously showed that calorie restriction ameliorated Huntington's disease pathogenesis and slowed disease progression in mice that model Huntington's disease (Huntington's disease mice)[1]. We now report that overexpression of sirtuin 1 (Sirt1), a mediator of the beneficial metabolic effects of calorie restriction, protects neurons against mutant HTT toxicity, whereas reduction of Sirt1 exacerbates mutant HTT toxicity. Overexpression of Sirt1 improves motor function, reduces brain atrophy and attenuates mutant-HTT–mediated metabolic abnormalities in Huntington's disease mice. Further mechanistic studies suggested that Sirt1 prevents the mutant-HTT–induced decline in brain-derived neurotrophic factor (BDNF) concentrations and the signaling of its receptor, TrkB, and restores dopamine- and cAMP-regulated phosphoprotein, 32 kDa (DARPP32) concentrations in the striatum. Sirt1 deacetylase activity is required for Sirt1-mediated neuroprotection in Huntington's disease cell models. Notably, we show that mutant HTT interacts with Sirt1 and inhibits Sirt1 deacetylase activity, which results in hyperacetylation of Sirt1 substrates such as forkhead box O3A (Foxo3a), thereby inhibiting its pro-survival function. Overexpression of Sirt1 counteracts the mutant-HTT–induced deacetylase deficit, enhances the deacetylation of Foxo3a and facilitates cell survival. These findings show a neuroprotective role for Sirt1 in mammalian Huntington's disease models and open new avenues for the development of neuroprotective strategies in Huntington's disease.

Alteration of cellular metabolism has a crucial role in the pathogenesis of Huntington's disease[2–4], raising the possibility of developing therapeutic interventions in Huntington's disease that activate metabolic defenses. Sirt1 is an evolutionarily conserved protein with NAD^+-dependent deacetylase activity that participates in cellular metabolism[5]. Sirt1 has neuroprotective roles in models of neurodegenerative diseases[6]. Whether Sirt1 has a protective role in mammalian Huntington's disease remains unknown, however, as results from lower organisms such as *Caenorhabditis elegans*[7] and *Drosophila melanogaster*[8] are contradictory.

To determine the role of Sirt1 in mammalian Huntington's disease models, we took advantage of a Sirt1 transgenic mouse model in which the expression of *Sirt1* is driven by a prion protein promoter[9]. Mice in this model strongly overexpress Sirt1 in the brain (**Fig. 1a**), although we also observed detectable concentrations of the Sirt1 transgene in peripheral tissues (**Fig. 1b**). As the first step in our experiment, we crossed these Sirt1 transgenic mice with N171-82Q Huntington's disease mice that have progressive phenotypes that resemble those in humans with Huntington's disease[1,10]. Sirt1 overexpression significantly delayed the onset and slowed the progression of motor deficits in Huntington's disease mice (**Fig. 1c**) without decreasing mutant HTT concentrations (**Supplementary Fig. 1a**). To determine whether improved motor function correlated with the progression of the neuropathological process, we performed an *in vivo* structural magnetic resonance imaging (MRI) analysis[11]. We detected significant atrophy in the striatum ($P < 0.05$) and neocortex ($P < 0.05$) of N171-82Q Huntington's disease mice, which resembled the neuropathological changes seen in human Huntington's disease. Overexpression of Sirt1 significantly attenuated the magnitude of brain atrophy (**Fig. 1d–f**). These results show that increased expression of Sirt1 attenuates neurodegeneration and improves motor function in N171-82Q Huntington's disease mice.

Having shown that overexpression of Sirt1 is protective in a Huntington's disease mouse model expressing an N-terminal mutant HTT fragment (fragment HD model), we then aimed to confirm these effects of Sirt1 in a Huntington's disease mouse model expressing full-length mutant HTT (full-length HD model). BACHD mice have motor deficits and Huntington's disease–like brain pathology

A full list of author affiliations appear at the end of paper.

Received 12 January; accepted 14 October; published online 18 December 2011; doi:10.1038/nm.2558

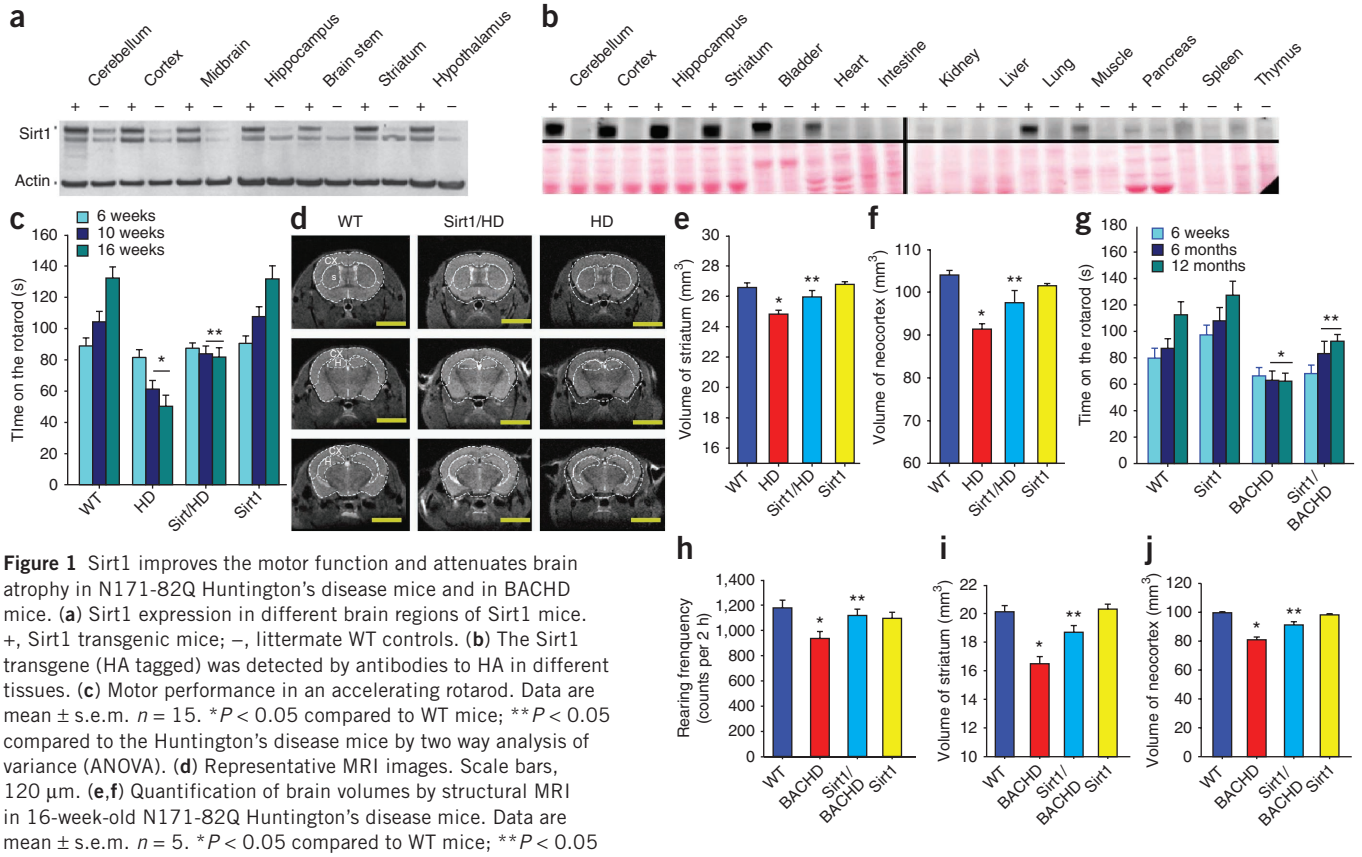

Figure 1 Sirt1 improves the motor function and attenuates brain atrophy in N171-82Q Huntington's disease mice and in BACHD mice. (**a**) Sirt1 expression in different brain regions of Sirt1 mice. +, Sirt1 transgenic mice; –, littermate WT controls. (**b**) The Sirt1 transgene (HA tagged) was detected by antibodies to HA in different tissues. (**c**) Motor performance in an accelerating rotarod. Data are mean ± s.e.m. $n = 15$. $^*P < 0.05$ compared to WT mice; $^{**}P < 0.05$ compared to the Huntington's disease mice by two way analysis of variance (ANOVA). (**d**) Representative MRI images. Scale bars, 120 µm. (**e**,**f**) Quantification of brain volumes by structural MRI in 16-week-old N171-82Q Huntington's disease mice. Data are mean ± s.e.m. $n = 5$. $^*P < 0.05$ compared to WT mice; $^{**}P < 0.05$ compared to Huntington's disease mice by ANOVA followed by Scheffé's *post-hoc* analysis. (**g**) Motor performance in an accelerating rotarod. Data are mean ± s.e.m. $n = 15$. $^*P < 0.05$ compared to WT mice; $^{**}P < 0.05$ compared to BACHD mice by two way ANOVA. (**h**) Rearing frequency in an open field assay in 15-month-old BACHD mice. Data are mean ± s.e.m. $n = 15$. (**i**,**j**) Brain volumes measured by MRI in 15-month-old BACHD mice. Data are mean ± s.e.m. $n = 5$. $^*P < 0.05$ compared to WT mice; $^{**}P < 0.05$ compared to BACHD mice by ANOVA followed by Scheffé's *post-hoc* analysis (**h**–**j**).

relatively earlier than mice from other available full-length Huntington's disease models[12,13]. Overexpression of Sirt1 significantly attenuated motor deficits (**Fig. 1g**,**h**) without decreasing the expression of mutant HTT (**Supplementary Fig. 1b**). Brain atrophy was partially ameliorated by Sirt1 overexpression (**Fig. 1i**,**j**), suggesting that Sirt1 also attenuates neurodegeneration in BACHD mice.

We previously showed that N171-82Q Huntington's disease mice have metabolic abnormalities that are attenuated by calorie restriction[1]. Therefore, we examined whether Sirt1 could modulate metabolic alterations in Huntington's disease mice. Overexpression of Sirt1 significantly ($P < 0.05$) attenuated hyperglycemia (**Supplementary Fig. 2a**), improved glucose tolerance (**Supplementary Fig. 2b**,**c**) and attenuated weight loss in N171-82Q Huntington's disease mice (**Supplementary Fig. 2d**). To determine whether the attenuation of weight loss was a result of the effect of Sirt1 on food intake, energy expenditure or both, we used Oxymax metabolic cages to measure energy expenditure continuously for a week and monitored daily food intake, and we found that Sirt1 counteracted the negative effect of mutant HTT on food intake (**Supplementary Fig. 2e**) but did not affect energy expenditure (**Supplementary Fig. 2f**). Notably, insulin concentrations did not differ between N171-82Q Huntington's disease mice and wild-type (WT) control mice (315.4 ± 51.5 pg ml^{-1} in WT mice compared to 308.9 ± 34.4 pg ml^{-1} in Huntington's disease mice (mean ± s.e.m.), $n = 10$), but Huntington's disease mice had hyperglycemia, suggesting insulin resistance in these mice. As insulin resistance constitutes a metabolic stressor that may contribute to the neurological phenotype, we next examined the role of Sirt1 on insulin concentrations. Sirt1 overexpression did not alter insulin concentrations in control mice (318.6 ± 83.7 pg ml^{-1} in mice overexpressing Sirt1 compared to 315.4 ± 51.5 pg ml^{-1} in WT mice (mean ± s.e.m.), $n = 10$) but did substantially reduce insulin concentrations in Huntington's disease mice (308.9 ± 34.4 pg ml^{-1} in Huntington's disease mice compared to 149.1 ± 6.8 pg ml^{-1} in Huntington's disease mice overexpressing Sirt1 (mean ± s.e.m.), $n = 10$). Sirt1 decreased insulin concentrations and attenuated hyperglycemia in Huntington's disease mice, indicating that Sirt1 improves insulin sensitivity in these mice. To determine whether overexpression of Sirt1 in brain, pancreas or both contributes to this effect, we examined the Sirt1 transgene expression pattern. Whereas the Sirt1 transgene is highly expressed in various brain regions (**Supplementary Fig. 3a**), we detected very low expression of it in the pancreas (**Supplementary Fig. 3b**). Although these results suggest a central action for Sirt1 in mediating metabolic rescue, the effects of Sirt1 on the pancreas cannot be completely ruled out.

Notably, Sirt1 overexpression did not extend life span in N171-82Q Huntington's disease mice (with an average life span of 152 ± 7 d in 19 Huntington's disease mice compared to 157 ± 6 d in 26 Huntington's disease mice overexpressig Sirt1 (mean ± s.e.m.)). Similar findings have been noted in other studies of mice that model Huntington's disease, in which reductions in neuropathology and improvements in motor function or normalization of glucose concentrations were observed in the absence of life span extension[14–17]. In addition, Sirt1 overexpression

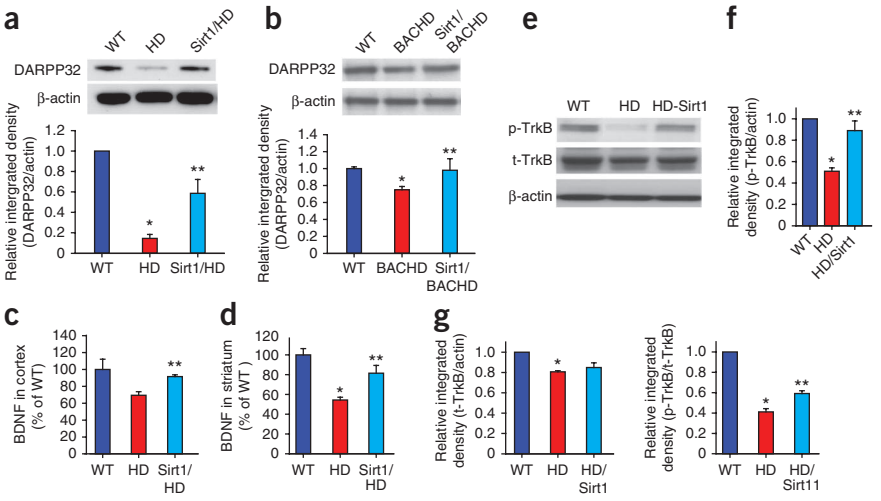

Figure 2 Sirt1 preserves DARPP32 concentrations in the striatum, restores BDNF concentration and facilitates TrkB activation in Huntington's disease models. (**a**,**b**) Sirt1 restored DARPP32 concentrations in N171-82Q Huntington's disease mice (**a**) and BACHD mice (**b**). At the top are representative western blots, and at the bottom are densitometry results. Sirt1/HD represents samples from N171-82Q HD mice overexpressing Sirt1, and Sirt1/BACHD represents samples from BACHD mice overexpressing Sirt1. $n = 4$. (**c**,**d**) BDNF protein concentrations were measured in cerebral cortex (**c**) or striatum (**d**) of 14-week-old N171-82Q Huntington's disease (HD) mice, wild-type controls (WT) and N171-82Q Huntington's disease mice overexpressing Sirt1 (Sirt1/HD). $n = 3$–6. (**e**) Representative western blots of total Trk-B (t-TrkB) and phosphorylated TrkB (p-TrkB) in immortalized striatal cells expressing wild-type HTT (WT) or mutant HTT (HD) and mutant HTT-expressing cells transfected with Sirt1 (HD-Sirt1). (**f**) Quantification of p-TrkB concentraitons from a densitometry analysis of the western blots. $n = 3$. At the top are the results as ratio of p-TrkB to β-actin; at the bottom are the results as ratio of p-TrkB to total TrkB. (**g**) Quantification of total TrkB concentraitons. $n = 3$. All data are mean ± s.e.m. $^*P < 0.05$ compared to WT mice; $^{**}P < 0.05$ compared to Huntington's disease mice by ANOVA followed by Scheffé's *post-hoc* analysis (**a**–**g**).

did not alter aggregation of mutant HTT (**Supplementary Fig. 4**), suggesting that aggregation of this mutant protein does not have a major role in the neuroprotective effects of Sirt1 in our models. Although Jeong *et al.* report that Sirt1 attenuates brain atrophy in R6/2 mice, suggesting a neuroprotective effect of Sirt1, they also saw increased survival and decreased aggregation of mutant HTT after overexpression of Sirt1 in R6/2 mice[18]. Notably, we showed that N171-82Q mice develop hyperglycemia and insulin resistance, which was not seen in their R6/2 model. There is a complicated relationship between insulin signaling and neurodegeneration. Whereas some reports suggest that reduced insulin signaling is protective in the central nervous system[19], others suggest the opposite[19]. Further studies will be required to determine the relationship between insulin resistance and survival in our model. However, we emphasize that the combined data of both studies show Sirt1-mediated striatal neuroprotection indicated by reduced striatal atrophy in two different fragment models and in a full-length mouse model of Huntington's disease, strongly suggesting a neuroprotective role for Sirt1 in Huntington's disease.

Next we determined the molecular basis underlying neuroprotection by Sirt1 in Huntington's disease. Huntington's disease mice are severely impaired in their ability to regulate the physiological state of striatal neurons through dopamine[20]. DARPP32 is a fundamental component of the dopamine signaling cascade[21,22], and Huntington's disease pathology is marked by extensive loss of medium spiny neurons that have high expression DARPP32; therefore, DARPP32 can serve as a marker of neuronal loss as well as of neuronal dysfunction in Huntington's disease[23,24]. We observed a significant reduction of DARPP32 concentrations in both the N171-82Q and BACHD mouse models (**Fig. 2a**,**b**), which is consistent with findings from other Huntington's disease mouse models[20]. Notably, Sirt1 restored DARPP32 concentrations in both the N171-82Q and BACHD Huntington's disease mouse models (**Fig. 2a**,**b**), suggesting that Sirt1 may protect striatal neurons against mutant HTT by preservation of DARPP32 concentrations.

Our previous study suggests that calorie restriction increases BDNF concentrations, thereby protecting neurons from the effects of mutant HTT[1]. Reduced BDNF concentration contributes to striatal dysfunction and degeneration, and an increase in BDNF concentration is neuroprotective in Huntington's disease[25]. BDNF signaling in the brain also has a crucial role in regulating glucose metabolism[26]. BDNF is required for the normal expression of DARPP32 (ref. 27). BDNF concentrations were significantly decreased in our fragment Huntington's disease model mice, whereas overexpression of Sirt1 markedly restored BDNF concentrations in the fragment HD model (**Fig. 2c**,**d**). In addition, we found that total TrkB and phospho-TrkB concentrations were significantly decreased in a striatal cell line containing mutant HTT (**Fig. 2e**,**f**). However, overexpression of Sirt1 maintained the concentration of phospho-TrkB but not total TrkB (**Fig. 2e**–**g**). These experiments suggest that Sirt1-mediated restoration of BDNF concentrations and of its prosurvival signaling might be a mechanism for Sirt1 neuroprotection in Huntington's disease.

Because our data suggest that overexpression of Sirt1 has neuroprotective effects in Huntington's disease models, we next sought to determine the role of endogenous Sirt1 in mutant-HTT–induced toxicity. We showed that complete knockdown of Sirt1 led to cell death in the absence of mutant HTT (data not shown), suggesting a role for Sirt1 in neuronal survival. Partial knockdown of Sirt1 (**Fig. 3a**) that was not toxic at baseline led to exacerbation of mutant-HTT–induced toxicity in differentiated PC12 cells inducibly expressing a mutant N-terminal HTT fragment (**Fig. 3b**). Together, these results indicate that endogenous Sirt1 has a neuroprotective role and that deficiency of Sirt1 in neurons increases the toxicity of mutant HTT.

Next, we asked whether Sirt1 deacetylase activity is required for its neuroprotection in Huntington's disease. We used a PC12 cell model in which inducible expression of mutant HTT caused cell toxicity[28]. We introduced Sirt1 expression by retroviral transduction (**Fig. 3c**,**d**). Overexpression of Sirt1 significantly reduced mutant-HTT–induced toxicity, as indicated by a decrease in lactate dehydrogenase (LDH) release (**Fig. 3e**) and an increase in AlamarBlue reduction (**Fig. 3f**). The deacetylase-deficient Sirt1 mutant (H363Y)[29] completely eliminated the neuroprotective effects of Sirt1 in this cellular model (**Fig. 3e**,**f**), showing that Sirt1 deacetylase activity is required for neuroprotection.

As a deacetylase, Sirt1 is known to deacetylate and modulate the activity of key transcription factors, for example, PGC-1α (ref. 30),

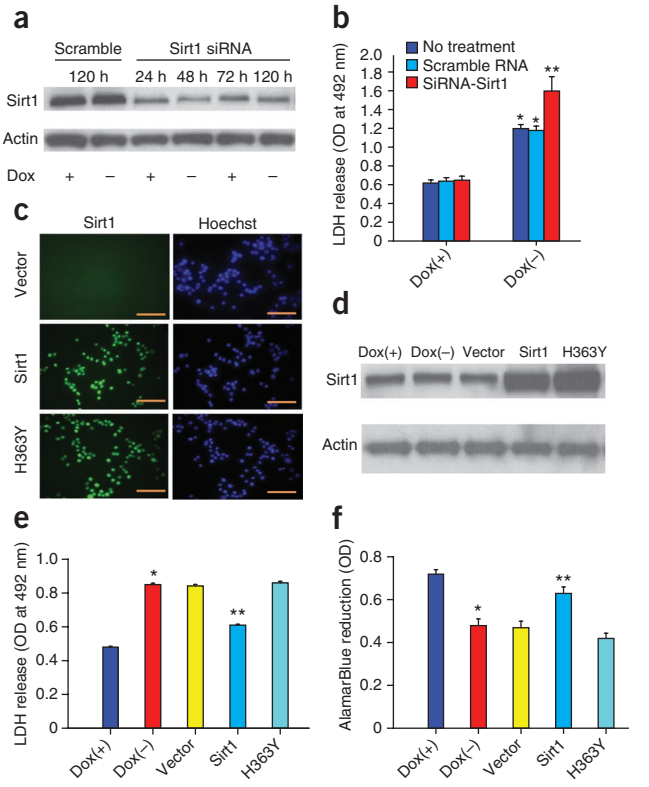

Figure 3 Ablation of endogenous Sirt1 exacerbates mutant HTT toxicity, and the deacetylase activity of Sirt1 is required for its neuroprotection in a cell model of Huntington's disease. (**a**,**b**) Reduction of Sirt1 exacerbates mutant-HTT–induced toxicity in a PC12 cell model inducibly expressing mutant HTT. Sirt1 protein concentrations were reduced by siRNAs (25 nM) (**a**), and reduction of Sirt1 concentration increased mutant-HTT–induced toxicity (**b**). Data are mean ± s.d. from three independent experiments. $*P < 0.05$ compared to the corresponding doxycycline-positive (Dox(+)) group; $**P < 0.05$ compared to the scramble RNA–treated doxycycline-negative (Dox(–)) group by ANOVA followed by Scheffé's *post-hoc* analysis. (**c**,**d**) Overexpression of Sirt1 or deacetylase-defective Sirt1 (H363Y) was introduced by retrovirus infection into a PC12 cell model inducibly expressing mutant HTT. Expression of Sirt1 was confirmed by immunostaining (**c**) and western blot analysis (**d**). Scale bars, 50 µm. (**e**,**f**) Mutant HTT expression was induced by withdrawal of doxycycline in nerve growth factor–differentiated PC12 cells. Overexpression of Sirt1 rescued mutant HTT–induced cell toxicity, indicated by reduction of LDH release (**e**) and AlamarBlue reduction (**f**) were measured. OD, optical density. Data are mean ± s.e.m. from three independent experiments. $*P < 0.05$ compared to the corresponding Dox(+) group; $**P < 0.05$ compared to the vector-transfected Dox(–) group by ANOVA followed by Scheffé's *post-hoc* analysis.

p53 (ref. 31) and Foxo3a[32]. Foxo3a is highly expressed in adult brain, and recent work indicates that Foxo3a has key roles in neuronal survival under both basal and disease conditions[33–35]. We detected an interaction between Sirt1 and Foxo3a in mouse brain (**Fig. 4a**). Notably, the concentrations of Foxo3a in Huntington's disease mouse brains and in striatal cells containing mutant HTT were significantly lower compared with those in wild-type control mouse brains or cells expressing normal HTT (**Fig. 4b**,**c**). Concentrations of acetylated Foxo3a that were significantly increased in cells containing mutant HTT (**Fig. 4d**) returned to baseline levels with overexpression of Sirt1 (**Fig. 4e**). In addition, overexpression of Sirt1 restored Foxo3a concentrations in the striatum of Huntington's disease mice (**Fig. 4b**) and in striatal cells containing mutant HTT (**Fig. 4c**). To examine whether Foxo3a contributes to the neuroprotection by Sirt1 in Huntington's disease, we used an immortalized striatal cell model. Cells containing mutant HTT were more vulnerable to serum withdrawal compared to cells containing normal HTT, as indicated by reduced ATP concentrations (**Fig. 4f** and **Supplementary Fig. 5a**). Sirt1 protected cells against mutant HTT, as indicated by a recovery of ATP concentrations (**Fig. 4f**). We further confirmed the neuroprotection of Sirt1 in cortical neurons transiently transfected with mutant HTT (**Supplementary Fig. 6**). Notably, reduction in the concentration of Foxo3a by RNAi knockdown compromised the protective effect of Sirt1 in striatal cells expressing full-length mutant HTT (**Fig. 4g**), suggesting that expression of Foxo3a is at least in part required for Sirt1-mediated neuroprotection.

Having shown that Foxo3a partially mediates the neuroprotection by Sirt1 in the striatal cell model of Huntington's disease, we asked whether restoring Foxo3a concentrations could protect cells from mutant HTT. Although restoring Foxo3a concentrations preserved ATP (**Supplementary Fig. 5b**), coexpression of Foxo3a and Sirt1 did not have an additive effect on ATP (**Supplementary Fig. 5c**). Next we examined a possible link between Foxo3a concentrations and mutant HTT-induced deficits of DARPP32 and BDNF. In the striatal cell model of Huntington's disease, overexpression of Foxo3a increased the concentrations of BDNF and DARPP32, whereas knockdown of Foxo3a further decreased DARPP32 concentrations (**Supplementary Fig. 7a–c**), suggesting that Foxo3a deficiency may contribute, either directly or indirectly, to mutant HTT-induced abnormalities in BDNF and DARPP32.

On the basis of these observations, we hypothesized that mutant HTT may influence Sirt1 deacetylase activity and thereby increase acetylation of its substrates. To examine this possibility, we first tested whether Sirt1 was able to interact with mutant HTT. Coimmunoprecipitation analyses revealed that Sirt1 interacted with mutant HTT (**Fig. 4h**). We then measured Sirt1 deacetylase activity. Using a specific antibody that detects acetylated p53 at Lys382, we found increased acetylation of p53 in HEK293 T/17 cells containing mutant HTT compared to cells containing WT HTT, suggesting that the mutant HTT interfered with Sirt1 deacetylase activity (**Fig. 4i**). In support of this notion, acetylated p53 was also increased in Huntington's disease mouse brains, whereas overexpression of Sirt1 led to decreased acetylation of p53 (**Fig. 4j**). Together, these experiments show that mutant HTT inhibits the deacetylase activity of Sirt1 and that overexpression of Sirt1 partially corrects the hyperacetylation of Sirt1 substrates.

In conclusion, we show a neuroprotective role for Sirt1 in cell and mouse models of Huntington's disease. Using both fragment and full-length HTT transgenic mouse models, we found that Sirt1 partially prevents neurodegeneration and ameliorates metabolic abnormalities in Huntington's disease mouse models. These results are in agreement with the accompanying paper, in which Sirt1-mediated neuroprotection was observed in an R6/2 Huntington's disease mouse model[18]. From a mechanistic standpoint, our data suggest that Sirt1 may regulate the activity of multiple targets, such as Foxo3a, DARPP32, BDNF and p53, to mediate neuroprotection in Huntington's disease models. Previous work showed that BDNF induces DARPP32 expression in medium spiny striatal neurons[27]. Our data also suggest that Foxo3a regulates DARPP32 and BDNF expression. Notably, we show that Sirt1 activity is inhibited by mutant HTT and that overexpression of Sirt1 overcomes this inhibition and regulates the acetylation of its substrates. Although we examined a subset of Sirt1 substrates in our models, it is

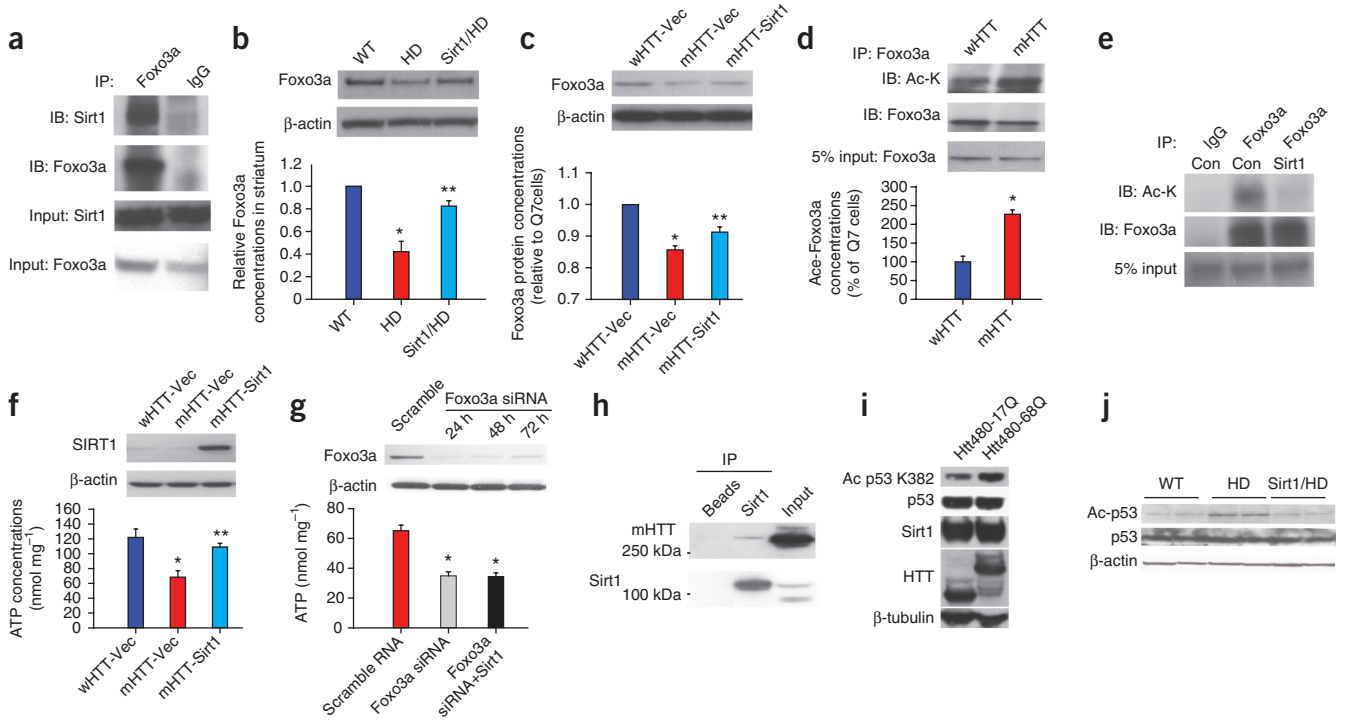

Figure 4 Sirt1 counteracts mutant-HTT–induced hyperacetylation of Foxo3a and p53 and protects cells against mutant-HTT–mediated energy deficits in both mouse and cell models of Huntington's disease. (**a**) Coimmunoprecipitation in mouse brains. (**b**) Foxo3a concentrations in striatum of 14-week-old mice. Data are mean ± s.e.m. $n = 4$. $^{*}P < 0.05$ compared to WT mice; $^{**}P < 0.05$ compared to Huntington's disease mice by ANOVA followed by Scheffé's *post-hoc* analysis. (**c**) Foxo3a concentrations in striatal cells expressing WT HTT ($STHdh^{Q7/Q7}$, wHTT) or mutant HTT ($STHdh^{Q111/Q111}$, mHTT) transfected with vector (Vec) and mutant-HTT–expressing cells transfected with *Sirt1* (mHTT-Sirt1). Data are mean ± s.e.m. from three independent experiments. $^{*}P < 0.05$ compared to wHTT-Vec cells; $^{**}P < 0.05$ compared to mHTT-Vec cells by ANOVA followed by Scheffé's *post-hoc* analysis. (**d**) Acetylated Foxo3a concentrations were quantified from three individual samples. $^{*}P < 0.01$ compared to wHTT cells by Student's *t* tests. (**e**) Deacetylated Foxo3a in striatal cells. $STHdh^{Q111/Q111}$ cells were transfected with vector (Con) or *Sirt1*. Acetylated-lysine, Ac-K. (**f**) ATP concentrations were measured by HPLC ultraviolet detection in an immortalized striatal cell model of Huntington's disease from the indicated groups. Data are mean ± s.e.m. $n = 3$. $^{*}P < 0.05$ compared to wHTT cells; $^{**}P < 0.05$ compared to mHTT-Vec cells by ANOVA followed by Scheffé's *post-hoc* analysis. (**g**) ATP concentrations were measured in the striatal cells transfected with scramble RNA, Foxo3a siRNA or Foxo3a siRNA and Sirt1 cDNA. The top image indicates Foxo3a protein content after the indicated transfection. Data are mean ± s.e.m. from three independent experiments. $^{*}P < 0.05$ compared to scrambled RNA–transfected cells. $^{*}P < 0.05$ compared to scrambled RNA–treated cells by ANOVA followed by Scheffé's *post-hoc* analysis. (**h**) Immunoprecipitation (IP) was conducted with antibody to Sirt1 in BACHD mouse cerebral cortex, and membranes were probed with MW1 antibody (top) that specifically recognizes mutant HTT, or antibody to Sirt1 (bottom). (**i**) p53 deacetylation at Lys382 was detected in HEK 293T/17 cells cotransfected with *Sirt1* and the indicated *HTT* cDNAs. Three independent experiments were performed, and a representative blot is shown. (**j**) Acetyl p53 and total p53 concentrations in the cerebral cortices of 18-week-old mice.

possible that inhibition of Sirt1 deacetylation by mutant HTT affects other unknown or known substrates. Indeed, Jeong *et al.* identified CREB regulated transcription coactivator 1 (TORC1) as a previously unknown target of Sirt1 deacetylase that regulates transcription of BDNF[18]. PGC-1α is also a substrate of Sirt1 and has been previously implicated in Huntington's disease pathogenesis[36–38]. It will be interesting to examine whether TORC1 is upstream of other Sirt1 targets, such as p53 and Foxo3a, and whether Sirt1 directly deacetylates several substrates in normal and diseased brain. Nonetheless, our data indicate that at least one of these substrates, Foxo3a, has a key role in mediating Sirt1 neuroprotection. Foxo3a has been also shown to control insulin sensitivity and influence energy metabolism[39,40]. Thus, modulation of Foxo3a by Sirt1 may also affect alterations in energy metabolism observed in Huntington's disease models.

Based on these results, we suggest that pharmacological targeting of Sirt1 to enhance its deacetylase activity may provide a new therapeutic opportunity for Huntington's disease. Small compounds with Sirt1 activation activity have been shown to be beneficial in experimental animals prone to metabolic diseases[41], and development of Sirt1 activators with high specificity and bioavailability may also be a promising approach for the treatment of Huntington's disease.

METHODS

Methods and any associated references are available in the online version of the paper at http://www.nature.com/naturemedicine/.

Note: Supplementary information is available on the Nature Medicine website.

ACKNOWLEDGMENTS

We thank L. Tsai at Massachusetts Institute of Technology for providing Sirt1 and H363Y retrovirus constructs, S. Imai at Washington University for providing Sir2 complementary DNAs (cDNAs), M. Macdonald at Harvard Medical School for providing $STHdh^{Q7/Q7}$ and $STHdh^{Q111/Q111}$ cells, S. Li and X. Li at Emory University for providing antibodies to EM48 and E. Waldron, C. Berlinicke, Y. Cheng and J. Jin at Johns Hopkins University School of Medicine for their technical assistance. This work was supported by the Hereditary Disease Foundation (W.D.), CHDI Foundation grant A-2120 (W.D.), NIH grant NS 16375 (C.A.R.), NIH grant NS35902 (D.M.H.), the NIA Intramural Research Program (B.M., H.C., S. Maudesley and M.P.M.), NIH grant R01NS051303 (D.K.), NIH grant EB003543 and ES012665 (S. Mori) and NIH grant NS065306 (J.Z.).

AUTHOR CONTRIBUTIONS

M.J. designed and conducted the experiments and interpreted the data. J.W. designed and conducted the experiments in BACHD mice. J.F. contributed to the cell culture experiments. L.D. and R.H.C. performed the HPLC assays. H.-K.J. and D.K. provided the acetylated-lysine antibody and conducted the Sirt1 deacetylase assay. T.W. and D.M.H. provided the Sirt1 mice and the Sirt1 tissue expression data. H.C. contributed to the immunohistochemistry. L.X. and Q.P. conducted behavioral tests. Z.H., J.Z. and S. Mori performed the MRI scans. T.S. and R.L.-C. contributed to the BDNF assays. N.A. carried out the primary neuronal assay. S.Z., K.S. and J.Q. contributed to the coimmunoprecipitation, cell counting and immunohistochemistry. K.L.K.T., S.A., T.H.M., B.M., S. Maudsley and M.P.M. contributed to the metabolic measurements and discussion. X.W.Y. provided the BACHD mice. C.A.R. helped with the conception, design and interpretation of the experiments. D.K. contributed to the discussion and helped with the writing of the paper. W.D. designed, directed and coordinated the project and wrote the paper.

COMPETING FINANCIAL INTERESTS

The authors declare no competing financial interests.

Published online at http://www.nature.com/naturemedicine/.
Reprints and permissions information is available online at http://www.nature.com/reprints/index.html.

1. Duan, W. *et al.* Dietary restriction normalizes glucose metabolism and BDNF levels, slows disease progression, and increases survival in huntingtin mutant mice. *Proc. Natl. Acad. Sci. USA* **100**, 2911–2916 (2003).
2. Ross, C.A. & Thompson, L.M. Transcription meets metabolism in neurodegeneration. *Nat. Med.* **12**, 1239–1241 (2006).
3. McGill, J.K. & Beal, M.F. PGC-1α, a new therapeutic target in Huntington's disease? *Cell* **127**, 465–468 (2006).
4. Browne, S.E. & Beal, M.F. Oxidative damage in Huntington's disease pathogenesis. *Antioxid. Redox Signal.* **8**, 2061–2073 (2006).
5. Haigis, M.C. & Sinclair, D.A. Mammalian sirtuins: biological insights and disease relevance. *Annu. Rev. Pathol.* **5**, 253–295 (2010).
6. de Oliveira, R.M., Pais, T.F. & Outeiro, T.F. Sirtuins: common targets in aging and in neurodegeneration. *Curr. Drug Targets* **11**, 1270–1280 (2010).
7. Parker, J.A. *et al.* Resveratrol rescues mutant polyglutamine cytotoxicity in nematode and mammalian neurons. *Nat. Genet.* **37**, 349–350 (2005).
8. Pallos, J. *et al.* Inhibition of specific HDACs and sirtuins suppresses pathogenesis in a *Drosophila* model of Huntington's disease. *Hum. Mol. Genet.* **17**, 3767–3775 (2008).
9. Satoh, A. *et al.* SIRT1 promotes the central adaptive response to diet restriction through activation of the dorsomedial and lateral nuclei of the hypothalamus. *J. Neurosci.* **30**, 10220–10232 (2010).
10. Schilling, G. *et al.* Intranuclear inclusions and neuritic aggregates in transgenic mice expressing a mutant N-terminal fragment of huntingtin. *Hum. Mol. Genet.* **8**, 397–407 (1999).
11. Zhang, J. *et al.* Longitudinal characterization of brain atrophy of a Huntington's disease mouse model by automated morphological analyses of magnetic resonance images. *Neuroimage* **49**, 2340–2351 (2010).
12. Gray, M. *et al.* Full-length human mutant huntingtin with a stable polyglutamine repeat can elicit progressive and selective neuropathogenesis in BACHD mice. *J. Neurosci.* **28**, 6182–6195 (2008).
13. Menalled, L. *et al.* Systematic behavioral evaluation of Huntington's disease transgenic and knock-in mouse models. *Neurobiol. Dis.* **35**, 319–336 (2009).
14. Li, M., Huang, Y., Ma, A.A., Lin, E. & Diamond, M.I. Y-27632 improves rotarod performance and reduces huntingtin levels in R6/2 mice. *Neurobiol. Dis.* **36**, 413–420 (2009).
15. Chopra, V. *et al.* A small-molecule therapeutic lead for Huntington's disease: preclinical pharmacology and efficacy of C2–8 in the R6/2 transgenic mouse. *Proc. Natl. Acad. Sci. USA* **104**, 16685–16689 (2007).
16. Chou, S.Y. *et al.* CGS21680 attenuates symptoms of Huntington's disease in a transgenic mouse model. *J. Neurochem.* **93**, 310–320 (2005).
17. Simmons, D.A., Mehta, R.A., Lauterborn, J.C., Gall, C.M. & Lynch, G. Brief ampakine treatments slow the progression of Huntington's disease phenotypes in R6/2 mice. *Neurobiol. Dis.* **41**, 436–444 (2011).
18. Jeong, H. *et al.* Sirt1 mediates neurprotection from mutant huntingtin by activation of the TORC1 and CREB transcriptional pathway. *Nat. Med.* advance online publication, doi:10.1038/nm.2558 (18 December 2011).
19. Cohen, E. & Dillin, A. The insulin paradox: aging, proteotoxicity and neurodegeneration. *Nat. Rev. Neurosci.* **9**, 759–767 (2008).
20. Bibb, J.A. *et al.* Severe deficiencies in dopamine signaling in presymptomatic Huntington's disease mice. *Proc. Natl. Acad. Sci. USA* **97**, 6809–6814 (2000).
21. Greengard, P., Allen, P.B. & Nairn, A.C. Beyond the dopamine receptor: the DARPP-32/protein phosphatase-1 cascade. *Neuron* **23**, 435–447 (1999).
22. Fienberg, A.A. *et al.* DARPP-32: regulator of the efficacy of dopaminergic neurotransmission. *Science* **281**, 838–842 (1998).
23. Vonsattel, J.P. *et al.* Neuropathological classification of Huntington's disease. *J. Neuropathol. Exp. Neurol.* **44**, 559–577 (1985).
24. de la Monte, S.M., Vonsattel, J.P. & Richardson, E.P. Jr. Morphometric demonstration of atrophic changes in the cerebral cortex, white matter, and neostriatum in Huntington's disease. *J. Neuropathol. Exp. Neurol.* **47**, 516–525 (1988).
25. Zuccato, C. & Cattaneo, E. Brain-derived neurotrophic factor in neurodegenerative diseases. *Nat. Rev. Neurol.* **5**, 311–322 (2009).
26. Nakagawa, T. *et al.* Brain-derived neurotrophic factor (BDNF) regulates glucose and energy metabolism in diabetic mice. *Diabetes Metab. Res. Rev.* **18**, 185–191 (2002).
27. Ivkovic, S., Polonskaia, O., Farinas, I. & Ehrlich, M.E. Brain-derived neurotrophic factor regulates maturation of the DARPP-32 phenotype in striatal medium spiny neurons: studies *in vivo* and *in vitro*. *Neuroscience* **79**, 509–516 (1997).
28. Wang, W. *et al.* Compounds blocking mutant huntingtin toxicity identified using a Huntington's disease neuronal cell model. *Neurobiol. Dis.* **20**, 500–508 (2005).
29. Kim, D. *et al.* SIRT1 deacetylase protects against neurodegeneration in models for Alzheimer's disease and amyotrophic lateral sclerosis. *EMBO J.* **26**, 3169–3179 (2007).
30. Rodgers, J.T. *et al.* Nutrient control of glucose homeostasis through a complex of PGC-1α and SIRT1. *Nature* **434**, 113–118 (2005).
31. Luo, J. *et al.* Negative control of p53 by Sir2α promotes cell survival under stress. *Cell* **107**, 137–148 (2001).
32. Morris, B.J. A forkhead in the road to longevity: the molecular basis of lifespan becomes clearer. *J. Hypertens.* **23**, 1285–1309 (2005).
33. Kops, G.J. *et al.* Forkhead transcription factor FOXO3a protects quiescent cells from oxidative stress. *Nature* **419**, 316–321 (2002).
34. Peng, K. *et al.* Knockdown of FoxO3a induces increased neuronal apoptosis during embryonic development in zebrafish. *Neurosci. Lett.* **484**, 98–103 (2010).
35. Mojsilovic-Petrovic, J. *et al.* FOXO3a is broadly neuroprotective *in vitro* and *in vivo* against insults implicated in motor neuron diseases. *J. Neurosci.* **29**, 8236–8247 (2009).
36. Cui, L. *et al.* Transcriptional repression of PGC-1α by mutant huntingtin leads to mitochondrial dysfunction and neurodegeneration. *Cell* **127**, 59–69 (2006).
37. Chaturvedi, R.K. *et al.* Impairment of PGC-1α expression, neuropathology and hepatic steatosis in a transgenic mouse model of Huntington's disease following chronic energy deprivation. *Hum. Mol. Genet.* **19**, 3190–3205 (2010).
38. Weydt, P. *et al.* Thermoregulatory and metabolic defects in Huntington's disease transgenic mice implicate PGC-1α in Huntington's disease neurodegeneration. *Cell Metab.* **4**, 349–362 (2006).
39. Tran, H. *et al.* DNA repair pathway stimulated by the forkhead transcription factor FOXO3a through the Gadd45 protein. *Science* **296**, 530–534 (2002).
40. Puigserver, P. *et al.* Insulin-regulated hepatic gluconeogenesis through FOXO1–PGC-1α interaction. *Nature* **423**, 550–555 (2003).
41. Milne, J.C. *et al.* Small molecule activators of SIRT1 as therapeutics for the treatment of type 2 diabetes. *Nature* **450**, 712–716 (2007).

[1]Division of Neurobiology, Department of Psychiatry and Behavioral Sciences, Johns Hopkins University School of Medicine, Baltimore, Maryland, USA. [2]Beijing Friendship Hospital, Capital Medical University, Beijing, China. [3]Natural Products Discovery Group, Department of Chemistry and Biochemistry, University of Oklahoma, Norman, Oklahoma, USA. [4]Department of Neurology, MassGeneral Institute for Neurodegenerative Disease, Massachusetts General Hospital, Harvard Medical School, Boston, Massachusetts, USA. [5]Department of Neurology and the Hope Center for Neurological Disorders, Washington University School of Medicine, St. Louis, Missouri, USA. [6]Department of Radiology, Johns Hopkins University School of Medicine, Baltimore, Maryland, USA. [7]Metabolism Unit, Laboratory of Clinical Investigation, National Institute on Aging (NIA), US National Institutes of Health (NIH), Baltimore, Maryland, USA. [8]Brain Mind Institute, Ecole Polytechnique Fédérale de Lausanne, Lausanne, Switzerland. [9]Department of Psychiatry and Behavioral Sciences, Brain Research Institute, University of California, Los Angeles, California, USA. [10]Department of Psychiatry and Behavioral Sciences, Johns Hopkins University School of Medicine, Baltimore, Maryland, USA. [11]Center for Metabolism and Obesity Research, Johns Hopkins University School of Medicine, Baltimore, Maryland, USA. [12]Laboratory of Neurosciences, NIA, NIH, Baltimore, Maryland, USA. [13]Department of Neuroscience, Johns Hopkins University School of Medicine, Baltimore, Maryland, USA. [14]Department of Neurology, Johns Hopkins University School of Medicine, Baltimore, Maryland, USA. [15]Department of Pharmacology, Johns Hopkins University School of Medicine, Baltimore, Maryland, USA. [16]Program in Cellular and Molecular Medicine, Johns Hopkins University School of Medicine, Baltimore, Maryland, USA. [17]These authors contributed equally to this work. Correspondence should be addressed to W.D. (wduan2@jhmi.edu).

ONLINE METHODS

Mice. We maintained N171-82Q Huntington's disease mice expressing N-terminal fragment HTT with a 82-polyglutamine repeat by breeding Huntington's disease males with C3B6F1 females (Taconic). As we reported previously[1], there are significant gender-dependent phenotype differences; therefore, we used all male N171-82Q mice for the study. BACHD mice expressing full-length mutant HTT were bred in an FVB background, and we used both male and female BACHD mice for the study. We obtained DNA from tails of the offspring of N171-82Q and BACHD mice for determination of the genotype and for CAG repeat size determination by PCR assay, which was performed by the Laragen genotyping service. The Sirt1 transgenic mouse line (line 1)[9] was generated by the overexpression of the hemagglutinin-tagged (HA tagged) *Sirt1* transgene driven by the mouse prion protein promoter (PrP). The *Sirt1* transgene (HA tagged) was constructed by inserting a 2.3-kb fragment of mouse *Sirt1* cDNA into the vector carrying the mouse PrP promoter after eliminating three NotI sites without changing the SIRT1 amino acid sequence and after adding the HA tag to the 3′ end of the *Sirt1* coding sequence. The PrP-*Sirt1*-HA transgene was linearized, purified and microinjected into C57BL/6J × CBA hybrid blastocysts in the Washington University Mouse Genetic Core Facility. We identified transgenic mice by PCR genotyping using tail DNA. Transgenic mice were backcrossed to C57BL/6 mice (Jackson Laboratories) for 6–7 generations before being imported to Johns Hopkins University. Nontransgenic littermates were used as controls. We generated mice by crossing Sirt1 heterozygotes with Huntington's disease heterozygotes to produce four genotypes: WT mice, Sirt1 transgenic mice, Huntington's disease mice and double transgenic mice (Sirt1/HD) for the current study. We housed the mice in groups of 3–5 mice with access to food and water *ad libitum* and a 12-h light and dark cycle. All animal protocols were approved by Institutional Animal Care and Use Committee at Johns Hopkins University.

***In vivo* MRI acquisition.** We performed *in vivo* MRI studies on a horizontal 9.4-T magnetic resonance scanner (Bruker Biospin, Billerica) with a triple-axis gradient and an animal imaging probe. The scanner was also equipped with a physiological monitoring system (with an electrocardiogram and monitoring of respiration and body temperature). Mice were anesthetized with isoflurane (1%) together with oxygen and air at a 1:3 ratio using a vaporizer and a facial mask. We used a 40-mm diameter birdcage coil for the radiofrequency transmitter and receiver. Temperature was maintained by a heating block built into the gradient system. We monitored respiration through the entire scan. We acquired images with a three-dimensional T2-weighted fast spin echo sequence with the following parameters: echo time (TE)/repetition time (TR) = 40/700 ms, resolution = 0.1 mm × 0.1 mm × 0.1 mm, echo train length = 4, number of average = 2 and flip angle = 40°. Mice recovered quickly once the anesthesia was turned off, and all mice survived the 50-min imaging sessions. The imaging resolution and contrast were sufficient for automatic volumetric characterization of the mouse brains and substructures. The detailed image analysis was described in our previous study[11].

ELISA analysis of BDNF protein concentrations. We quantified BDNF protein concentrations with a commercially available kit (Chemicon). Briefly, we processed samples by acidification and a subsequent neutralization. Wells of 96-well plates were coated with antibody to BDNF. Samples (300 µg of protein) were added to triplicate wells, and serial dilutions of BDNF standard (0–500 pg ml^{-1}) were added to the wells to generate a standard curve. We washed the wells five times with washing buffer, and after addition of streptavidin enzyme and substrate, reactions were stopped by adding 100 µl of HCl stop solution. We measured the absorbance at 450 nm using a plate reader. We determined the concentrations of BDNF in each sample in triplicate and used the average of the three values as the value for that mouse.

Inducible PC12 cells' expression of mutant HTT and the cell toxicity assay. PC12 cells inducibly expressing mutant HTT were generated as previously described[28]. We maintained cells in the presence of doxycycline (200 ng ml^{-1}), and the medium was changed every 48 h. Sirt1 siRNA or a retrovirus containing *Sirt1* was introduced after cells attached to the plate, and we measured cell toxicity and viability at 72 h after induction of mutant HTT. A Cytotoxicity Detection Kit (Roche) was used for the measurement of LDH. We used AlamarBlue reduction for the cell viability assay.

Sirt1 deacetylase activity. For the p53 deacetylation assay, we co-transfected HEK T/17 cells with *Sirt1* and HTT480-17Q or HTT480-68Q and treated the cells with 500 nM trichostatin A (TSA) to inhibit class I and class II HDACs and 100 µM etoposide to induce the expression of endogenous p53 for 6 h. At 24 h after transfection, we harvested cells and analyzed for p53 acetylation by western blotting with antibody to acetylated p53 at Lys382.

Immunoprecipitation. We analyzed acetylated Foxo3a concentrations using immunoprecipitation with antibody to Foxo3a followed by western blotting with antibody to acetyl lysine. We obtained cell extracts by incubating with 10 mM nicotinamide, 1 µM TSA and 500 µM H_2O_2 for 1 h and lysing in Radioimmunoprecipitation assay (RIPA) buffer (Sigma) containing deacetylase inhibitors (10 mM nicotinamide and 1 µM TSA), protease inhibitors and phosphatase inhibitors (Sigma). Foxo3a was immunoprecipitated with antibody to Foxo3a (1:2,000; Sigma). We detected the concentrations of total Foxo3a and acetylated Foxo3a using antibody to Foxo3a or monoclonal antibody to acetyl lysine (1:1,000 dilution). For the Foxo3a and Sirt1 interaction assay, we lysed mouse striatal samples in RIPA buffer (Sigma) containing protease inhibitors (Sigma). We immunoprecipitated tissue lysates using antibody to Foxo3a for 12 h and then washed extensively with RIPA buffer, and probed membranes with antibody to Sirt1 (1:10,000; Upstate) or antibody to Foxo3a.

Western blot analysis. We separated solubilized proteins by SDS-PAGE and transferred them to a nitrocellulose membrane. We incubated the membrane with primary antibodies (Bcl-X_L, 1:200, Santa Cruz; Sirt1, 1:10,000, Upstate; DARPP32, 1:2,000, Chemicon; p-TrkB, 1:100, Santa Cruz; Foxo3a, 1:2,000, Sigma; and β-actin, 1:5,000, Sigma). We then exposed the membrane for 1 h to horseradish peroxidase–conjugated secondary antibody (1:3,000; Jackson ImmunoResearch Labs Inc.) and visualized the proteins by using a chemiluminescence-based detection kit (ECL kit; Amersham).

Nucleotide extraction and HPLC assay. Conditionally immortalized striatal cell lines expressing wild-type HTT ($STHdh^{Q7/Q7}$) or mutant HTT ($STHdh^{Q111/Q111}$) cells, which were a gift from M. MacDonald at Harvard Medical School, were used in this study. We cultured cells in DMEM (Gibco) supplemented with 4% FBS (HyClone), 2 mM L-glutamine (Mediatech Inc.) and 100 units ml^{-1} penicillin and 100 units ml^{-1} streptomycin (Mediatech Inc.). We grew the cells at 33 °C in a humidified atmosphere containing 5% CO_2. We measured ATP concentrations by HPLC analysis with ultraviolet detection. Briefly, the cell pellets (about one million cells) were washed twice in cold PBS (pH 7.4). We extracted nucleotides with 50 µl of ice-cold acetonitrile followed by 150 µl of cold water followed by centrifugation at 14,000*g* for 10 min at −2 °C. We transferred the supernatant fraction into a new 1.5-ml tube, which was kept on ice, and the solvent was partially evaporated with N_2 for 15–20 min to remove the acetonitrile. We solubilized the cell pellets and analyzed the protein content using the bicinchoninic acid protein assay kit (Pierce). We performed an HPLC analysis on a Shimadzu system using a SCL-10A VP system controller and ZORBAX 3.5-µm SB-C18 column (4.6 nm × 150 mm) with flow rate of 0.8 ml per min. The samples were analyzed using an isocratic mobile phase consisting of 0.05 mol l^{-1} $NH_4H_2PO_4$ (pH 5.7) and an injection volume of 20 µl. The detection wavelength was set at 257 nm. We used HPLC-grade nucleotide standards to calibrate the signals, and the recovery rate exceeded 90% for ATP, ADP and AMP. We quantified all data using LCsolution software (Shimadzu) and normalized the ATP concentrations by protein content.

Statistical analyses. We used two-way (genotype and age) repeated ANOVA to calculate differences in longitudinal behavioral results and body weight data and one-way or two way ANOVA with a Scheffé *post hoc* test to calculate the differences in all other data among the groups. All the cell culture experiments were repeated independently at least three times. The significance between groups was determined using an ANOVA followed by *post-hoc* analysis between two groups. Data were analyzed with SIGMASTAT version 3.1 software.

Additional methods. Detailed methods, including the mutant HTT inclusion assay, blood glucose measurement, energy expenditure, behavioral tests and the survival study are described in the **Supplementary Methods**.

Supplementary Fig. 1

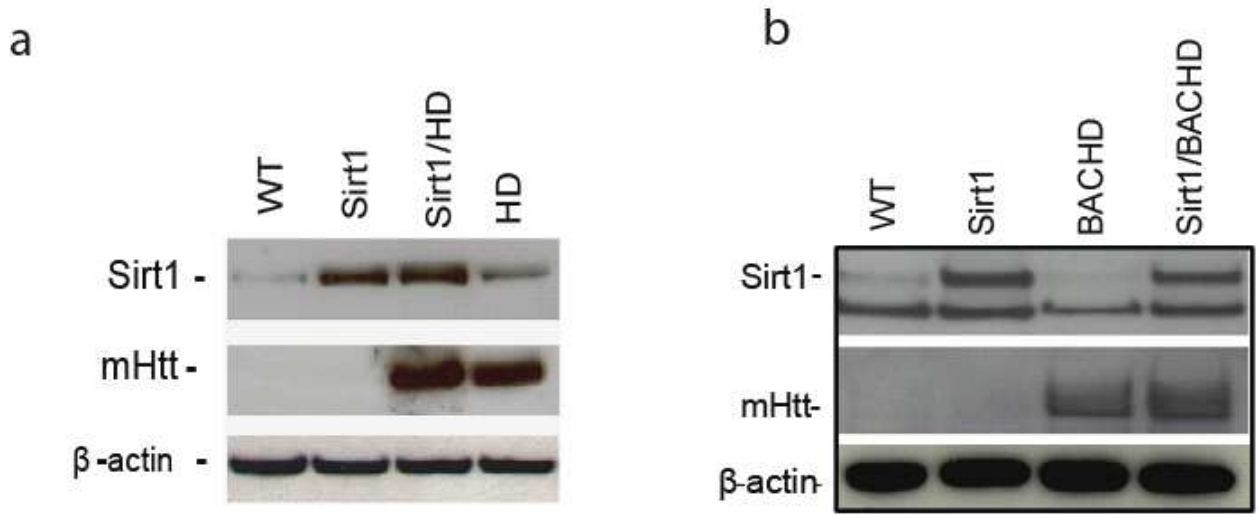

Supplementary. Fig. 1. (**a**) Sirt1 and mutant HTT (detected by HTT 81-90 antibody) protein levels were detected by Western blotting in cerebral cortex of N171-82Q mice. (**b**) Sirt1 and mutant HTT (detected by 1C2 antibody) protein levels were detected by Western blotting in cerebral cortex of BACHD mice.

Supplementary Fig. 2

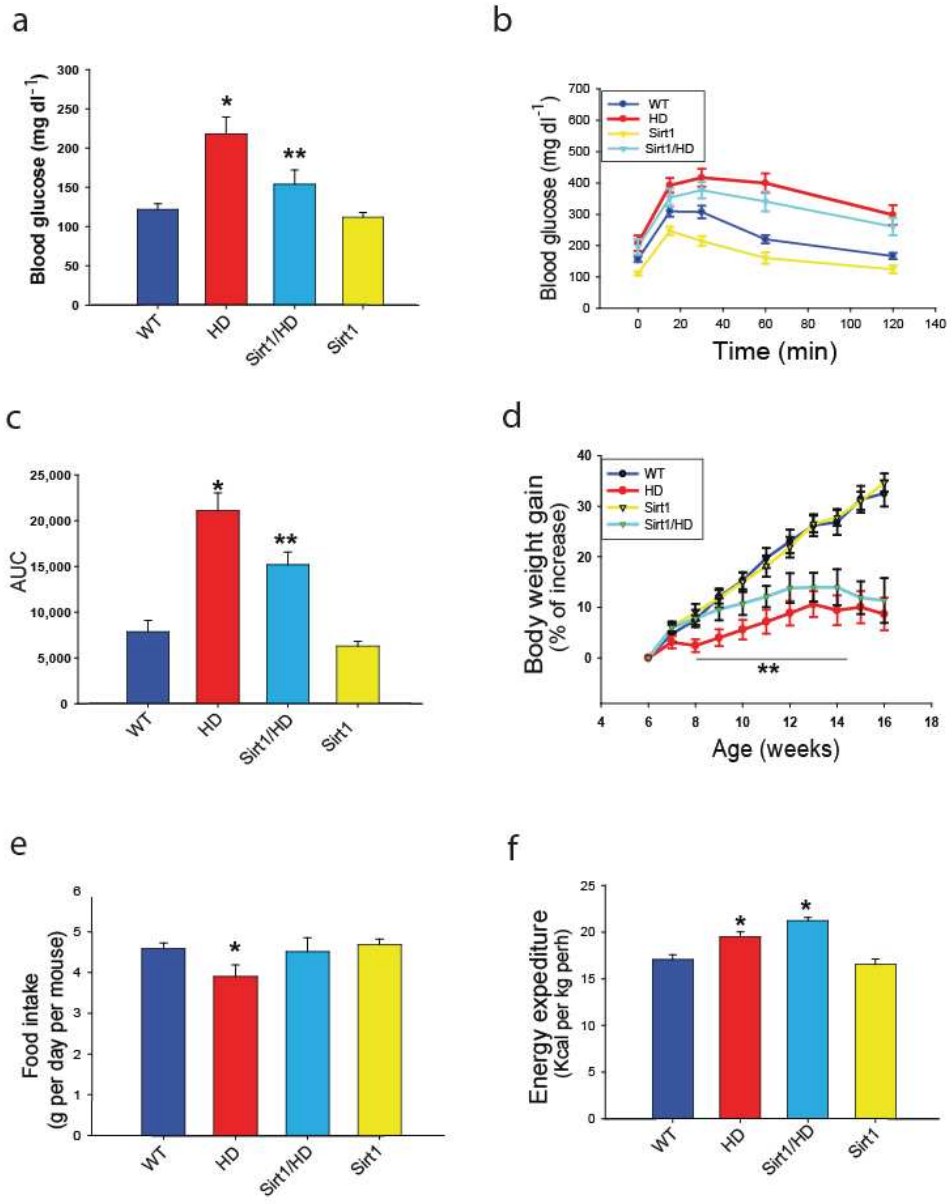

Supplementary Fig. 2. Sirt1 improves glucose tolerance and regulates energy metabolism in N171-82Q HD mice. (**a**) Blood glucose levels were measured after an overnight fast in 14-week-old mice. Mean ± S.E.M., *n*=10. (**b-c**) Mice were fasted overnight and then administered D-glucose (1g/kg, i.p); blood samples were taken before and at indicated times after glucose administration. The absolute values (b) and area under curve (AUC) (c). *n*=12. Mean ± S.E.M. (**d-f**) Effects of Sirt1 overexpression on body weight (d), food intake (e), energy expenditure (f) measured by an Oxymax metabolic system at 16 weeks old mice. Mean ± S.E.M.. *n*=12. **p*<0.01 compared with the value of wild type (WT); ***p*<0.05 compared with the value of HD.

Supplementary Fig. 3

a

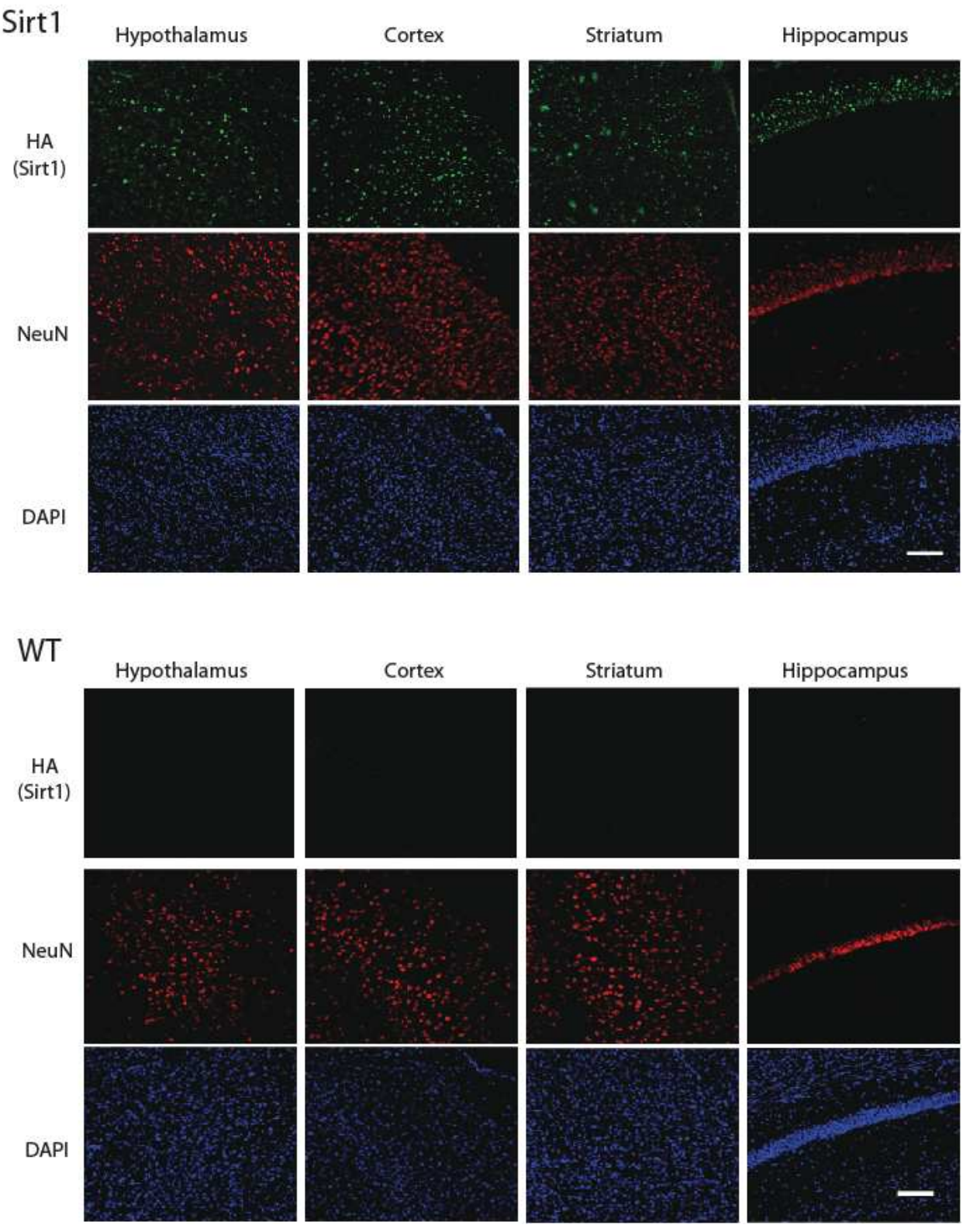

Nature Medicine doi:10.1038/nm.2558

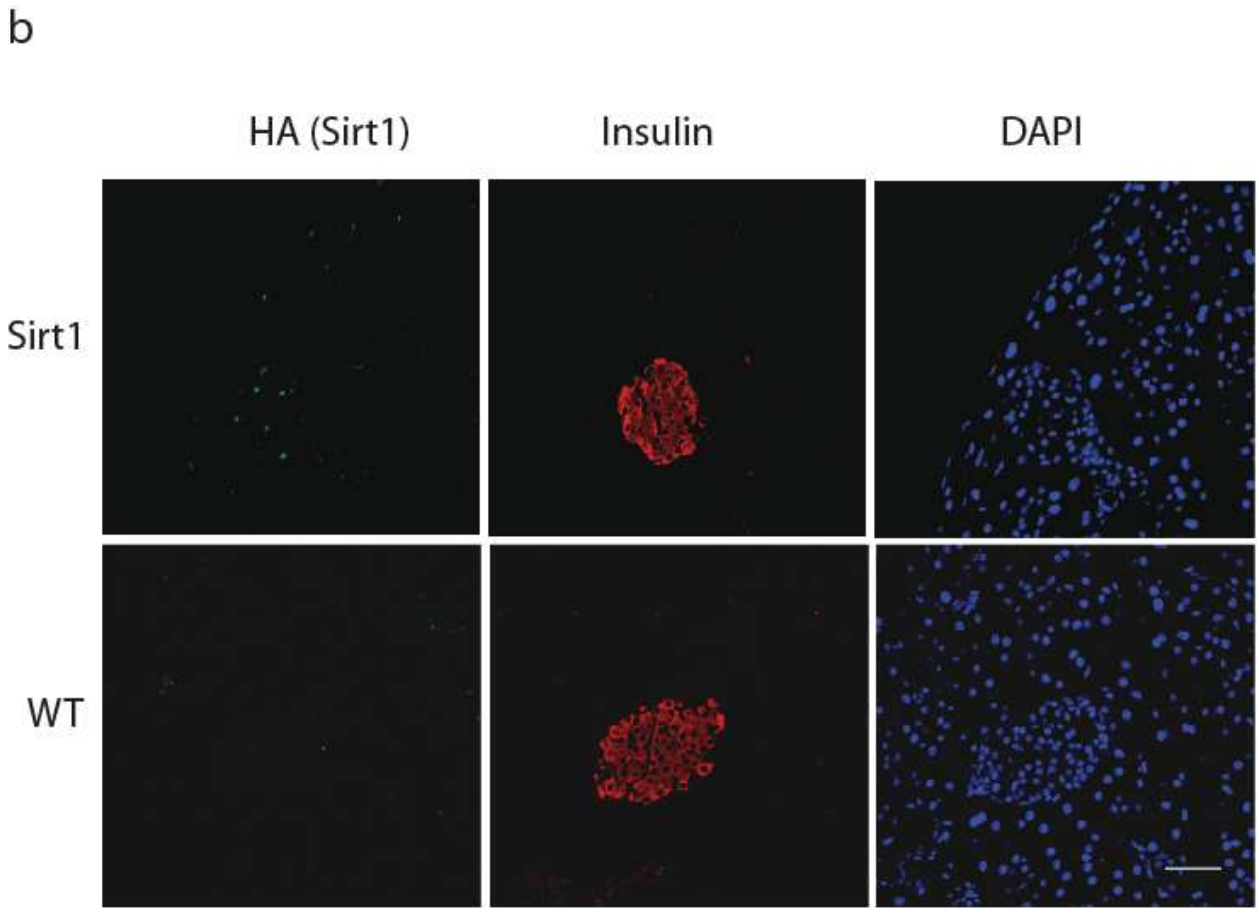

Supplementary Fig. 3 Transgene Sirt1 is highly expressed in the brain and barely detectable in the pancreas by immunofluorescent staining in Sirt1 transgenic mice. (**a**) Representative pictures of immunofluorescent staining of transgene Sirt1 (HA-tagged, green), NeuN staining (red), and DAPI in different brain regions from a Sirt1 trangenic mouse (Sirt1) and a wild type control mouse (WT). Scale bar 100 μm. (**b)** Representative pictures of immunofluorescent staining of transgene Sirt1 (HA, green), insulin (red), and DAPI (blue) in pancreatic islets of Langerhans from a Sirt1 transgenic mouse (Sirt1) and a wild type littermate control (WT). Scale bar 50 μm.

Supplementary Fig. 4

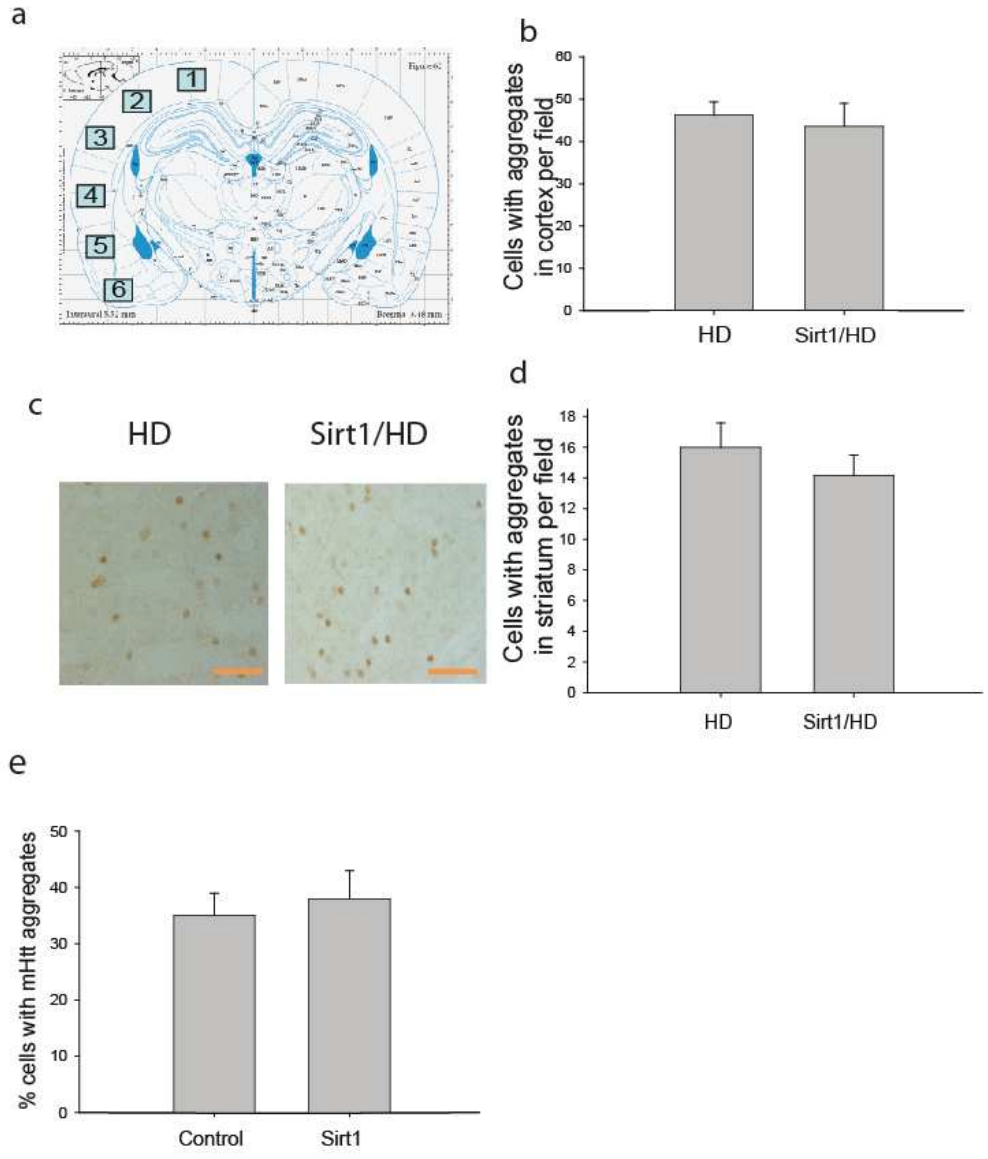

Supplementary Fig. 4. Sirt1 has no effects on mutant HTT aggregates in N171-82Q HD mice. (**a**) Diagram shows the areas of the cortex that were evaluated for HTT aggregates. (**b**) Average number of cells with mutant HTT aggregates in the cerebral cortex of mice in each microscope field. (**c**) Representative images from striatum immunostained with EM48 antibody. Scale bars 50 μm. (**d**) Average number of cells with mutant HTT aggregates in the striatum of mice in each microscope field. Mean ± S.E.M. from 5 mice per group. (**e**) N-terminal mutant HTT (N63-148Q-myc) expression was induced by withdrawal of doxycycline from the medium, and Sirt1 overexpression was introduced by retrovirus at the same time as mutant HTT induction. Cells were fixed for immunofluorescent staining at 48 h after induction of mutant HTT expression. Mutant HTT was labeled with myc antibody (myc-tagged N63-148Q). Mean ± S.E.M. from three independent experiments.

Supplementary Fig. 5

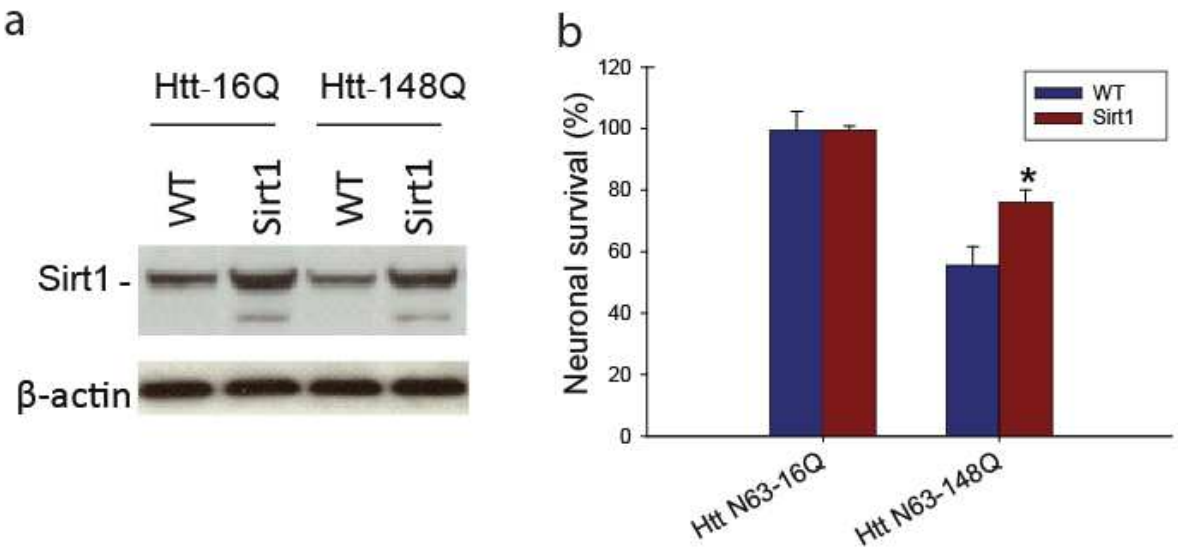

Supplementary Fig. 5. **Sirt1 increases neuronal resistance to mutant HTT toxicity**. (**a**) Primary cortical neurons were cultured from Sirt1 transgenic mice or wild type (WT) control mice. Levels of Sirt1 in primary cortical neurons were detected by Western blotting. (**b**) Neurons overexpressing Sirt1 are more resistant to mutant HTT-induced neurotoxicity. Cortical neurons were cultured from Sirt1 transgenic mice or wild type control mice, and transfected with mutant *HTT* (Htt-N63-148Q) or normal *HTT* (Htt-N63-16Q) fragment at DIV5, and neuronal survival was assessed at 48 h after transfection by nuclear DNA morphology. The numbers of surviving neurons in transfected neurons were measured. *$p<0.05$ *vs* the value of WT neurons transfected with HTT-N63-148Q.

Supplementary Fig. 6

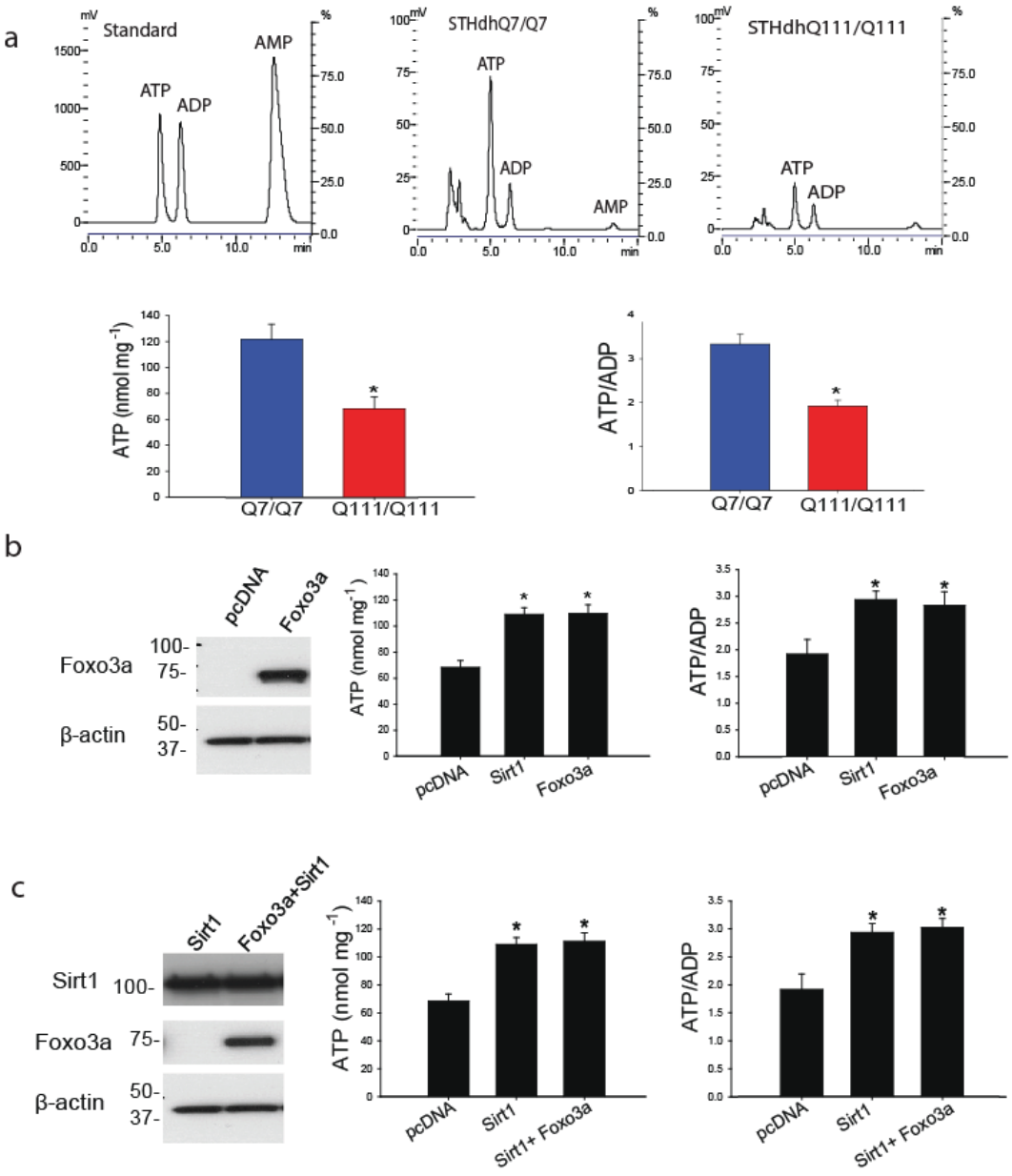

Supplementary Fig. 6. Effects of Foxo3a and Sirt1 on mutant HTT-induced ATP deficits in STHdh $^{Q111/Q111}$ cells. **(a)** HPLC chromatograms showing adenosine nucleotides ATP, ADP, and AMP in wild-type STHdh $^{Q7/Q7}$ and quantification data showing decreased ATP levels as well as ATP/ADP ratio in mutant STHdh $^{Q111/Q111}$ cells. (**b**) Increase in Foxo3a had similar protective effects as Sirt1 on mutant HTT-induced ATP deficits in STHdh $^{Q111/Q111}$ cells. (**c**) Effects of overexpression of Foxo3a and Sirt1 on mutant HTT-induced energy deficits in STHdh $^{Q111/Q111}$ cells. Mean ± S.E.M from three independent experiments. *p<0.05 *vs* the values of pcDNA vector-transfected group by Student's *t*-tests.

Supplementary Fig. 7

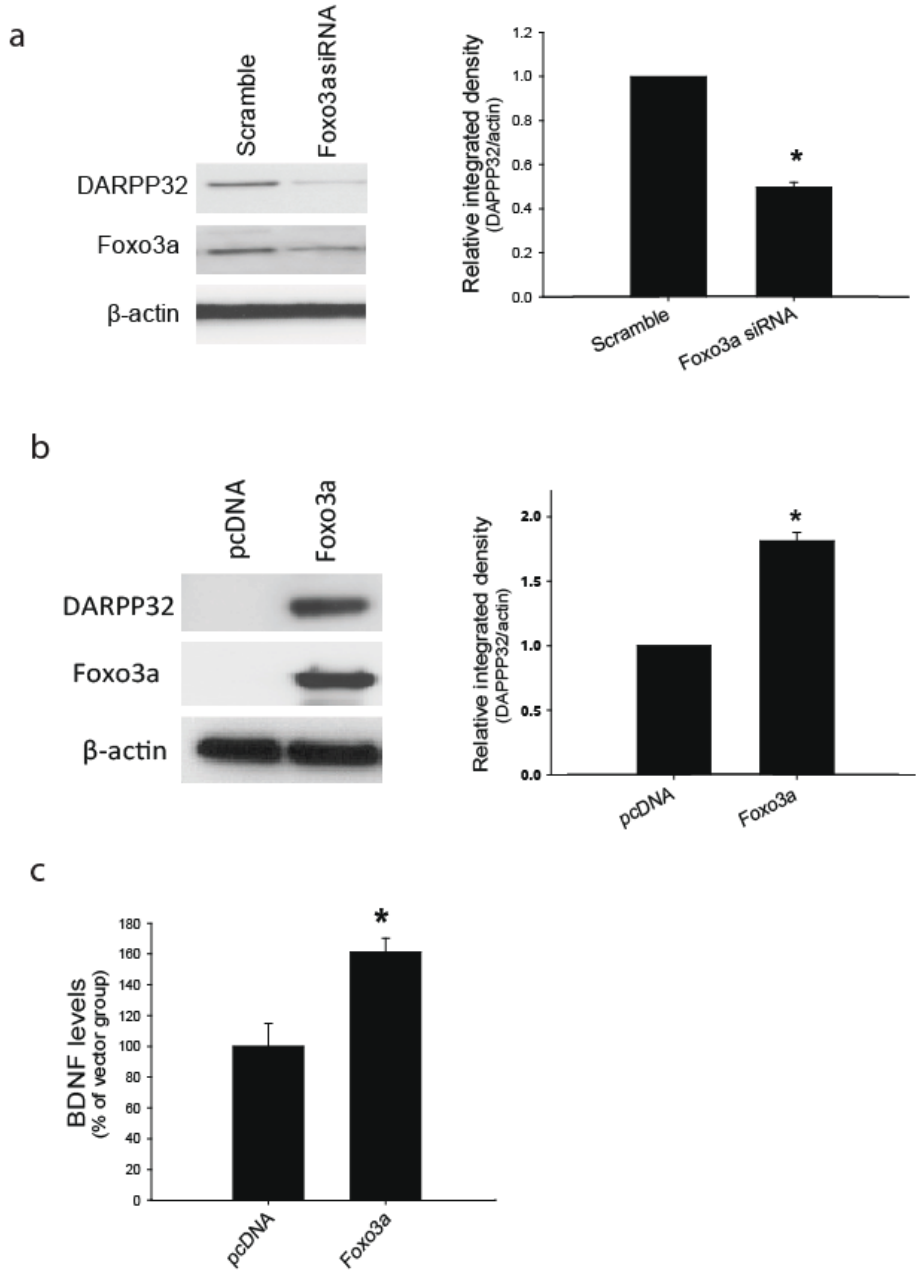

Supplementary Fig. 7. Foxo3a regulates levels of DARPP32 and BDNF levels in cells expressing mutant HTT (STHdh $^{Q111/Q111}$ cells). (**a**) Knockdown of Foxo3a by siRNA decreased DARPP32 levels in STHdh $^{Q111/Q111}$ cells. Foxo3a siRNA or scramble controls were transfected into STHdh $^{Q111/Q111}$ cells and DARPP32 levels were determined at 24 h after transfection. *p< 0.01 *vs* scramble RNA transfected group. (**b-c**) Overexpression of Foxo3a increased levels of DARPP32 (b) and BDNF (c) in STHdh $^{Q111/Q111}$ cells. Foxo3a cDNA or vector control (pc DNA) was transfected into cells, and levels of DARPP32 and BDNF were determined at 48 h after transfection. *p<0.05 *vs* pc DNA vector group by Student's *t*-tests.

Supplementary Methods

Mutant HTT aggregates immunostaining Brain sections were cut at 40 μm and immunostained with an EM48 antibody (mouse monoclonal antibody 1:100. a gift from S. Li and X. Li at Emory University), which preferentially recognizes mutant HTT aggregates. The cell numbers with mutant HTT inclusions in the striatum and cortex were counted by a person blinded to the groups. N63-148Q PC12 cells were transduced with Sirt1 retrovirus, 48 h after transduction, cells were fixed by 4% paraformaldehyde and immunofluorescent staining was carried out with following antibodies to c-myc (for mutant HTT, as N63-148Q is myc tagged, 1:300, Oncogene), Sirt1 (1:1000, Upstate Inc.). Pictures were taken and percentage of cells with mHTT aggregates was calculated.

Foxo3a overexpress/siRNA STHdh cells were planted in 6-well plates at the day before transfection. Cells were then transfected with Lipofectamine TM 2000 (Invitrogen) according to the manufacturer's instructions. Briefly, 2 μg Foxo3a pcDNA plasmid (Addgene) and 4 μl Lipofectamine TM 2000 were diluted in 250 μl of Opti-MEM medium respectively. For Foxo3a siRNA (Sigma), 200 pmol/well RNA and 4 μl/well Lipofectamine TM 2000 were diluted in 250 μl of Opti-MEM medium, respectively. After incubation for 5 min, DNA or siRNA and Lipofectamine TM 2000 were mixed and incubated for 20 min at room temperature. 500 μL of the mixture of DNA or RNA and LipofectamineTM2000 were added to cultures. The maintenance medium DMEM containing FBS was replaced at 4 h after transfection.

Coimmunoprecipitation for detecting mutant HTT and Sirt1 interaction BACHD mouse brain tissues were lysed in RIPA buffer (cell signaling) containing protease inhibitors (Sigma) on ice for 30 min. After adding 2 times volume of PBS, tissue lysates were immunoprecipitated using antibody to Sirt1 (1:1000, Upstate,) overnight, then washed with RIPA/PBS (1:2) buffer, and membranes were blotted with MW1 antibody (1:10000, gift from Dr. Paul H. Patterson) and antibody to Sirt1 (1:10000, Upstate).

Immunofluorescent staining in pancreas Animals were anesthetized using inhalation isoflurane (~1ml/430cm^3) before euthanization by decapitation. The pancreas was collected from each animal and fixed in formalin for 8-10 hours and then transferred into phosphate buffered saline (PBS). Subsequently, the pancreata were embedded in paraffin and sectioned at 5μm thickness. Pancreas sections were immunostained as described previously (Martin et al., 2009). Briefly, after antigen retrieval with citrate buffer (Invitrogen, Carlsbad, CA) at 98°C for 20 minutes, sections were blocked in 5% bovine serum albumin (BSA; Sigma, St. Louis, MO) for 1 hour, followed by incubation with insulin (1:500; Sigma) and SIRT(HA) (1:1000) antibodies diluted in 1% BSA overnight at 4°C. Subsequently, after washing in PBS, sections were incubated for 1 hour with fluorescent secondary antibodies (Alexa 488, Alexa 568, 1:1000, Invitrogen), and nuclei were counterstained with DAPI. No fluorescent staining was observed in any sections when primary antibodies were omitted. Images were collected using a confocal microscope LSM-710 (Carl Zeiss).

Blood glucose and insulin levels Mice were fasted overnight and blood samples were collected by venipuncture. Blood glucose concentrations were measured with a glucometer (Lifescan Inc, Milpitas, CA). The glucose tolerance test was performed on mice following an overnight fast: mice were given D-glucose (1g/kg, i.p), and the blood glucose concentration was measured in samples taken at 0, 15, 30, and 120 min after glucose administration. Serum insulin levels were measured by ELISA (Crystal Chem).

Energy expenditure Mice were initially housed (up to 1 week) in ventilated caging (Innovive) adapted to the local light:dark cycle. Mice were then weighed and moved to individual chambers of an Oxymax indirect calorimeter (Columbus Instruments). The chambers (4 x 8 x 7) are Lucite, with stainless steel or plastic floors. Daily body weight and food intake were monitored while the mice remained in the Oxymax. Energy production can be estimated by measuring the amount of O_2 consumed (i.e., oxidative phosphorylation). For fat and carbohydrates, this information comes from the respiratory exchange ratio (RER). RER is the ratio of VCO_2/VO_2 per unit of time.

Behavioral tests and Survival study Survival was monitored daily by two experienced operators (M. Jiang and Q. Peng). The mice were considered to be at the end of life when HD mice were unable to right themselves after being placed on their backs and initiate movement after being gently prodded for 30 sec. Motor behavioral performance was assessed with a rotarod apparatus (Columbus Instruments). The open field box was divided into 25 squares (5 × 5 cm each, San Diego Instrument). The mice were allowed to habituate for 10 min and then their activity was recorded for the following 10 min. The number of squares that the mice entered during the last 2 min of the recording session was determined. This short time at the end of the session was chosen in order to increase the habituation period, during which the activity is increased in normal animals because of their exploratory behavior. This increase in activity is the greatest during the first 20 min in a new environment.

Nature Medicine doi:10.1038/nm.2558